Chemical Reduction of SIM MOX in Molten Lithium Chloride Using Lithium Metal Reductant

Tetsuya Kato[a], Tsuyoshi Usami[a], Masaki Kurata[a], Tadashi Inoue[a], Howard E. Sims[b], and Jan A. Jenkins[c]

[a] Nuclear Technology Research Laboratory, Central Research Institute of Electric Power Industry, 2-11-1 Iwado-kita, Komae-shi, Tokyo 201-8511, Japan
[b] Nexia Solutions, Harwell, Didcot, Oxon, UK
[c] AEA Technology plc., Harwell, Didcot, Oxon, UK

Reprint requests to T. K.; Fax: +81-3-3480-7956; E-mail: tkato@criepi.denken.or.jp

Z. Naturforsch. **62a,** 513 – 523 (2007); received April 11, 2007

Presented at the EUCHEM Conference on Molten Salts and Ionic Liquids, Hammamet, Tunisia, September 16 – 22, 2006.

A simulated spent oxide fuel in a sintered pellet form, which contained the twelve elements U, Pu, Am, Np, Cm, Ce, Nd, Sm, Ba, Zr, Mo, and Pd, was reduced with Li metal in a molten LiCl bath at 923 K. More than 90% of U and Pu were reduced to metal to form a porous alloy without significant change in the Pu/U ratio. Small fractions of Pu were also combined with Pd to form stable alloys. In the gap of the porous U-Pu alloy, the aggregation of the rare-earth (RE) oxide was observed. Some amount of the RE elements and the actinoides leached from the pellet. The leaching ratio of Am to the initially loaded amount was only several percent, which was far from about 80% obtained in the previous ones on simple MOX including U, Pu, and Am. The difference suggests that a large part of Am existed in the RE oxide rather than in the U-Pu alloy. The detection of the RE elements and actinoides in the molten LiCl bath seemed to indicate that they dissolved into the molten LiCl bath containing the oxide ion, which is the by-product of the reduction, as solubility of RE elements was measured in the molten LiCl-Li_2O previously.

Key words: Pyrometallurgical Reprocessing; Lithium Reduction Process; Actinoides; Uranium-Plutonium Mixed Oxide; Molten Salt.

1. Introduction

The Central Research Institute of Electric Power Industry (CRIEPI) in Japan has been developing the pyrometallurgical reprocessing of spent metallic fuel [1], which was originally proposed by the Argonne National Laboratory (ANL) [2]. Molten salt electrorefining is the main step in reprocessing to recover actinoides, i. e. uranium (U), plutonium (Pu), and minor actinoides. Actinoides in the fuel alloy are dissolved anodically into the molten salt and reduced to metal at the cathodes for selective recovery [3 – 6]. The reduction process of the spent oxide fuel was also proposed by the ANL, aiming to apply the molten salt electrorefining to the reduced metallic material [7]. One of the techniques is called lithium (Li) reduction, in which Li metal is used as the reductant. The spent oxide fuel is reduced in a bath of molten lithium chloride (LiCl), because the use of the mediating solvent is considered to encourage the reduction. The by-product of the reaction, lithium oxide (Li_2O), should dissolve up to the solubility of 8.8 wt% Li_2O in molten LiCl [8], and then diffuse in the solvent as to withdraw from the front region of the reaction. It is also an advantage for the reduction that the chemical activity of the by-product dissolving in the solvent is lower than a unit of solid Li_2O.

The authors have also been studying the Li reduction process and already carried out reduction experiments using actinoides. The dioxides of U, neptunium (Np), Pu, and americium (Am) were used in powder form individually, and then it was found that all of them were reduced to metal [8 – 10]. Another experiment was conducted with a MOX pellet containing U, Pu, and Am [11]. The reduced pellet remained intact to form the alloy, where lots of pores and cracks developed due to the significant decrease in the molar volume from the oxide to the metal. In those experiments with Pu and Am, it was found that a part of them leached from the bulk material.

Element	Starting material
U, Pu, Am	MOX pellet
Np	NpO_2 powder
Cm	Nitric acid solution containing Cm
Pd	PdO powder
Mo	MoO_2 powder
Zr	ZrO_2 powder
Ba	BaO powder
Sm	Sm_2O_3 powder
Ce	CeO_2 powder
Nd	Nd_2O_3 powder

Table 1. Starting material of each element contained in the SIM MOX.

This paper describes Li reduction experiments using a mixed oxide containing twelve elements: U, Pu, Am, Np, curium (Cm), palladium (Pd), molybdenum (Mo), zirconium (Zr), barium (Ba), samarium (Sm), cerium (Ce), and neodymium (Nd). The behaviour of the elements was examined in the multi-element system, especially focusing on the distribution behaviour of each element in the reduced material and the molten salt bath.

2. Experimental

2.1. Preparation of Simulated Spent Oxide Fuel

The mentioned twelve elements formed a mixed oxide to study the reduction by Li. The mixed oxide was called a simulated spent oxide fuel (SIM MOX). Table 1 indicates the starting material for preparing the SIM MOX. The starting material of U, Pu, and Am was the same MOX pellet as previously used [11]. All of the Am in the MOX pellet is produced by the β decay of Pu-241. The pellet was crushed in a mortar to particles of less than 200 μm size and mixed with the other starting materials. The starting material of Cm was a nitric acid solution containing 100 ppm of Cm. For the other elements, oxide powders were used. Small samples were taken from the mixture of the starting materials and dissolved in hot nitric acid containing 1 wt% of hydrofluoric acid to analyze the composition of the SIM MOX. Table 2 indicates the composition of the SIM MOX. Since the oxides of Pd, Mo, and Zr are difficult to dissolve into the acidic solution, their contents shown in Table 2 were nominal values calculated from the starting materials added. The content of U, Pu, and Am was almost same as in the previous experiment using the MOX [11]. Thus the result of this study was compared with that of the MOX pellet reduction to discuss the influence of the coexisting fission products on the distribution of U, Pu, and Am. A small content of Cm was required as a tracer. The content of other elements was determined by referring to the composition of a spent fuel. Table 2 also indicates the composition with burn-up of 48 GWd/t-U in PWR and a cooling time of 4 years, which was calculated by the ORIGEN-II code.

Element	Wt% in cations	
	SIM MOX	Spent fuel[a]
U	85.5[b]	94.7
Pu	10.3[b]	1.02
Am	0.16[b]	0.06
Np	0.45[b]	0.07
Cm	$6{\cdot}10^{-5}$ [b]	0.01
Pd	0.55[c]	0.24
Mo	0.54[c]	0.48
Zr	0.55[c]	0.50
Ba	0.52[b]	0.24
Sm	0.46[b]	0.12
Ce	0.50[b]	0.34
Nd	0.51[b]	0.58

Table 2. Composition of the SIM MOX.

[a] Calculated using ORIGEN-II code for PWR fuel, 48 GWd/t-U, and 4 years cooling time.
[b] Analyzed.
[c] Calculated from addition of starting material.

In the previous experiments using the MOX pellet, the reduced material remained in almost the original pellet form [11], therefore the SIM MOX in this study was also sintered into a pellet as to recover easily the reduced material from the molten salt bath using a mesh basket. The mixture of the starting materials was dried and put in a die with 10.6 mm inner diameter to fabricate a green pellet of 10 g. The pressure on the die was 5 metric tons. The sintering was carried out at 1773 K for 4 h in argon/3 wt% hydrogen. Three sintered pellets were prepared of almost the same size. One was used to observe the cross section before the Li reduction, and the others were for the reduction experiment conducted in two different conditions.

2.2. Procedure of Lithium Reduction

The reduction experiment was carried out twice in a glove box containing an argon atmosphere with less than 20 ppm of oxygen and moisture. The content of Li_2O in the molten salt bath influenced the behaviour of each element in the Li reduction. For instance, it was found that Am oxide was reduced to metal at a Li_2O content of less than 5 wt% [9], and that for rare-earth (RE) elements dissolved in molten LiCl-Li_2O the RE solubility increases with increasing Li_2O content [12]. Thus, considering that the Li_2O content would reach 2 wt% and 6 wt% at the end of the Li reduction, 100 g and 30 g of LiCl were used in RUN 1 and RUN 2, respectively. The initial molar ratios of (U+Pu)/LiCl were 0.0145 in RUN 1 and 0.0485 in RUN 2.

The weighed LiCl was contained in a tungsten crucible, placed in an electric furnace, and then heated up to 923 K. The sintered SIM MOX pellet was wrapped in a coarse tungsten mesh and immersed in the molten salt bath. The tungsten mesh was tied to a tungsten wire in order to pick up the reduced pellet above the molten salt level at the end of the reduction experiment. The molten salt bath was agitated with a tungsten stirrer rotating at 100 rpm. The stirrer was a tungsten rod with 10 mm diameter, of which the bottom end was obliquely cut to form a blade for the agitating action. The reductant Li metal was added to the molten salt bath incrementally. Before each addition, a sample was taken from the molten salt bath by freezing a small amount on a dipped steel rod. Each regular sample was lighter than 0.2 g to avoid a sudden decrease of the molten salt bath. At the end of the reduction, the reduced pellet was pulled up from the molten salt bath and cooled to ambient temperature in the furnace. The recovered pellet and the remnant in the crucible were analyzed to examine the distribution of each element.

2.3. Analysis

The regular salt sample was analyzed for the content of Li metal and the concentration of Li_2O as mentioned previously [8 – 11]. The sample was dissolved in water to measure the hydrogen that evolved by the reaction between Li metal and H_2O using a gas burette. The amount of LiOH, which generated from Li metal and Li_2O in the aqueous solution, was measured by titration. The contribution of Li metal was subtracted to determine the concentration of Li_2O in the molten salt bath. The aqueous solution was also analyzed for the twelve elements contained in the molten salt bath.

The recovered pellets were mounted in a resin and cut along the vertical axis of the cylindrical form. The cross section of the half piece was polished to examine the morphology and the local composition, using a scanning electron microscope (SEM) with an X-ray microanalyzer (XMA). The composition was determined using ZAF correction. The archive pellet was also cut and polished to observe the cross section.

The other half of the reduced pellets was cut into smaller pieces, and they were used for the determination of the reduction yield [8 – 11]. The sample was dissolved in hydrobromic acid to measure the hydrogen evolution using a gas burette. The metal content in the piece was calculated using the equations

$$\mathrm{U} + 4\mathrm{HBr} \rightarrow \mathrm{UBr_4} + 2\mathrm{H_2}, \tag{1}$$

$$\mathrm{Pu} + 3\mathrm{HBr} \rightarrow \mathrm{PuBr_3} + 3/2\mathrm{H_2}. \tag{2}$$

A pre-test with the gas burette was performed to show the applicability of the measurement. The hydrogen evolution was measured dissolving zinc (Zn), U, and Pu into hydrobromic acid. The result is summarized in Table 3 to show the theoretical and the experimental values of the hydrogen evolution at 273 K and 1 atm. The theoretical value was calculated applying (1) and (2) for U and Pu, and the following equation for Zn:

$$\mathrm{Zn} + 2\mathrm{HBr} \rightarrow \mathrm{ZnBr_2} + \mathrm{H_2}. \tag{3}$$

The experimental value for Zn, U, and Pu was consistent with the theoretical one. Thus, almost all of the hydrogen evolution was enclosed in the gas burette without major leakage, and (1) and (2) were representative of the hydrogen evolution from U and Pu dissolving in hydrobromic acid, respectively.

After the determination of the reduction yield, the aqueous solution was analyzed for the composition. The residue, which was left in the crucible after the Li reduction, was also dissolved in nitric acid and analyzed to examine the leaching of each element from the pellet. Among this leaching, the amount in the molten salt was determined by the analysis of samples taken from the molten salt bath just before the end of the Li reduction. The other amount of the leaching was regarded as the precipitate. Thus the material balance was examined, classifying under the three parts of the reduced pellet the molten salt and the precipitate on the crucible bottom.

Table 3. Result of the pre-test for the determination of the metal amount using a gas burette.

Sample metal	Mass / mg	H_2 evolution[a] / mL		Experimental / theoretical
		Theoretical	Experimental	
Zn	145	49.7	50.2	1.01
	121	41.4	41.1	0.99
U	90	16.9	16.1	0.95
	103	19.4	18.8	0.97
	79	14.9	14.5	0.97
	113	21.3	20.6	0.97
Pu	107	15.0	15.4	1.02
	96	13.5	13.8	1.02
	43	6.0	6.1	1.00
	139	19.5	19.7	1.01

[a] Volume at 273 K and 1 atm.

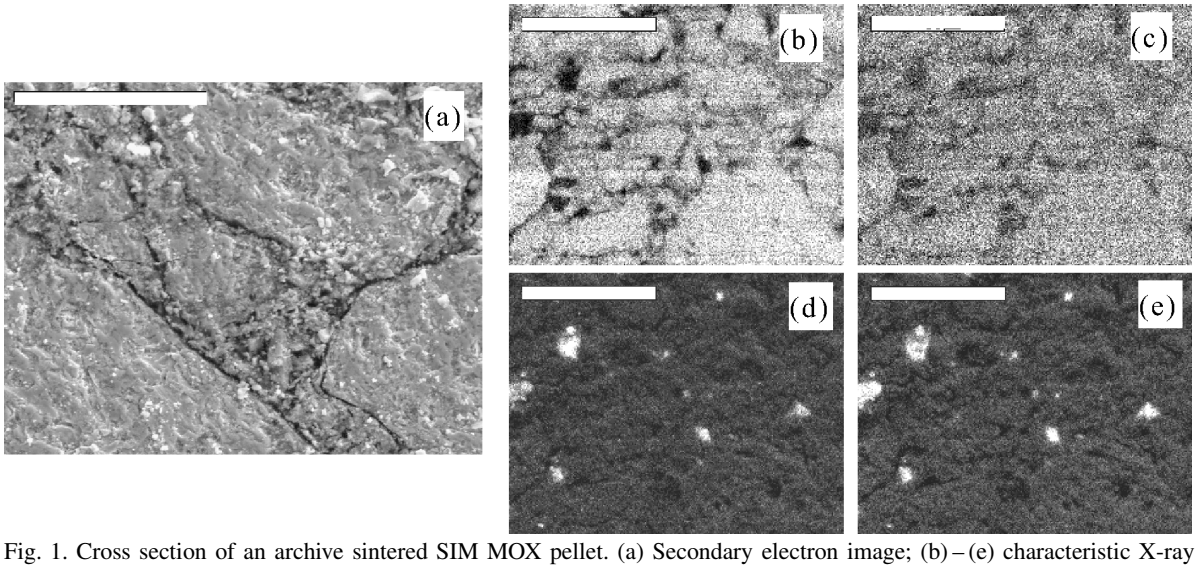

Fig. 1. Cross section of an archive sintered SIM MOX pellet. (a) Secondary electron image; (b) – (e) characteristic X-ray images of U, Pu, Zr, and Ba, respectively. The white bar in the figures indicates 50 μm in length.

The quantitative analyses for Pu, Am, and Np were carried out by means of γ-spectrometry [8 – 11]. For the determination of the Np content, the γ-ray from Pa-233, which is normally in radioactive equilibrium with Np-237, was measured. The measurement of Cm was carried out by α-spectrometry [13, 14]. Prior to the measurement, U, Pu, and Np were separated by using aqueous/organic extraction. The intensity of the α-ray emitted from Am as well as Cm was measured to obtain the yield during the preparation of the counting sample, and the content of Cm was corrected for the yield. The other elements were measured by inductively coupled plasma-atomic emission spectrometry (ICP-AES).

3. Results and Discussion

3.1. Observation of a Sintered SIM MOX Pellet

The sintered SIM MOX pellet of 10 g was in an approximate size of 10.8 mm diameter and 14 mm height. The density calculated from the weight and dimension was about 7.5 g/cm^3, which was much smaller than the theoretical density of UO_2, 11.0 g/cm^3 [15]. Figure 1a is the secondary electron image of the cross section of the archive pellet. Although gaps were observed between the grains, the pellets were consolidated firmly so as not to collapse by handling in the glove box.

The following features were observed on the SIM MOX. Figures 1b – e are the characteristic X-ray images of U, Pu, Zr, and Ba, respectively. The distribution of U and Pu was almost homogeneous, and the local weight ratio of Pu/U was obtained using XMA to be 0.109 ± 0.020. The value was consistent with 0.121 of the Pu/U ratio calculated from the composition indicated in Table 2. As shown in Fig. 1d and e, Zr and Ba formed an inclusion, of which the composition was examined by means of XMA. A major part of the inclusion, say more than 60 wt%, was Ba and Zr, of which the molar ratio scattered from 1 to 2 of Ba/Zr. Double oxides of Ba and Zr were considered to form even in the sintered SIM MOX pellet, since $BaZrO_3$ and Ba_2ZrO_4 are known as thermodynamically stable compounds [16]. Other local compositions were examined at random using XMA. Since a small amount of RE elements was detected in the matrix of U and Pu, RE elements diffused into the MOX matrix. The random analysis of the local compositions also revealed that there was a little amount of inclusion consisting of Mo and Pd mainly.

3.2. Increase of Li_2O in Molten LiCl by Li Reduction

The progress of the Li reduction was followed by analysis using a gas burette and titration to check the content of Li metal and Li_2O in the molten salt bath. The result of RUN 1 and RUN 2 is shown in Figs. 2a and b, respectively, with the horizontal axis of the cumulative Li metal addition. The open circles in Fig. 2 denote the Li metal content. The closed circles indi-

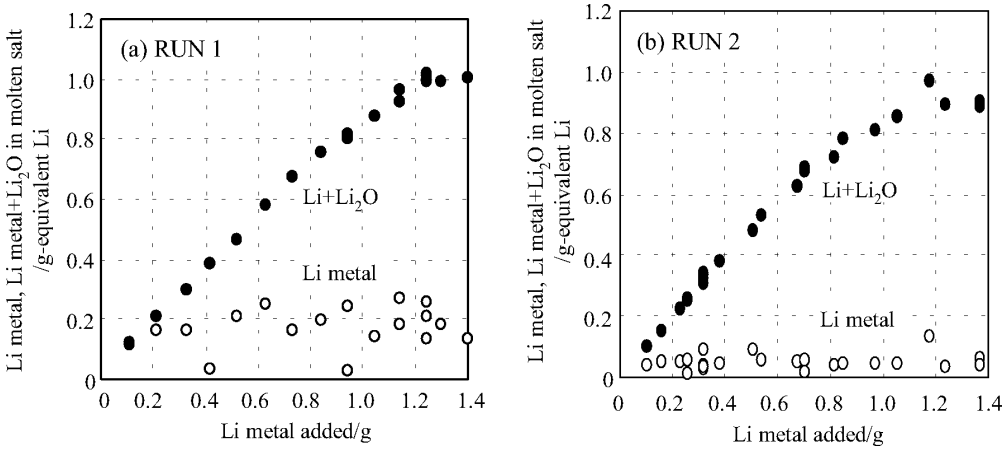

Fig. 2. Li metal (○) and Li+Li_2O (●) detected in the molten salt bath with respect to Li metal added. (a) RUN 1; (b) RUN 2.

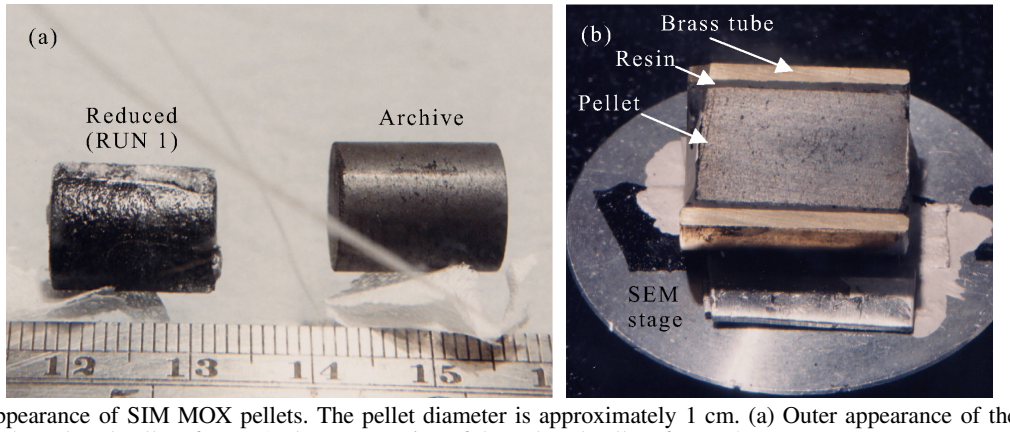

Fig. 3. Appearance of SIM MOX pellets. The pellet diameter is approximately 1 cm. (a) Outer appearance of the archive pellet and the reduced pellet of RUN 1; (b) cross section of the reduced pellet of RUN 2.

cate the total Li amount contributed by Li metal and Li_2O in the molten salt, which was determined by titration. Although the Li metal content scattered due to analytical error caused by the extremely small hydrogen evolution (less than 1 mL), it was roughly constant through the reduction experiments. Thus the contribution originated by Li metal to the titration was found to be limited.

The total Li amount of Li metal + Li_2O was in good agreement with the cumulative Li metal addition in the early stage of the reduction, but gradually diverged from the Li metal addition. Therefore, some of Li_2O appeared to have stayed inside the reduced material. The total Li amount increased with increasing the Li metal addition until the cumulative Li metal addition reached about 1.2 g, which was comparable to 1.0 g of Li metal required for the reduction of 10 g of UO_2. Since the Li metal added further did not contribute significantly to the increase of Li_2O detected in the molten salt bath but wetted on the tungsten stirrer, the reduction of the actinoide oxides was considered to have almost finished. The total Li amount finally reached 1.0 g in RUN 1 and 0.9 g in RUN 2, respectively. The final Li_2O content in the molten salt bath was determined using the salt samples of about 3 g, which gave larger hydrogen gas evolution and a more precise Li metal content than the regular samples. The values were (1.8 ± 0.06) wt% and (7.5 ± 0.13) wt% Li_2O in RUN 1 and RUN 2, respectively.

3.3. Measurement of the Reduction Yield

The pellet recovered after RUN 1 is shown in Fig. 3a together with the archive pellet. The pellets of both RUN 1 and RUN 2 did not collapse but remained intact. Figure 3b shows the cross section of the pellet of

Table 4. Reduction yield determined using a gas burette.

RUN No.	H_2 evolution[a] / mL	Metal mass / mg	Total mass of actinoides / mg	Reduction yield / %
RUN 1	45.1	246	272	90
	16.3	89	93	96
	23.0	126	131	96
RUN 2	48.4	265	282	94
	35.6	194	205	95
	18.0	98	104	95
	13.6	74	77	97

[a] Volume at 273 K and 1 atm.

RUN 2. The outer surface of the reduced pellets looked black but the cross section shiny metallic. Thus the reduction reaction was found to reach the center of the bulky material.

Small sample pieces were cut from various parts of the reduced pellets and used for the determination of the reduction yield. The sample was washed with water prior to dissolution in hydrobromic acid, since Li metal adhering to it contributes to the hydrogen evolution. The result is summarized in Table 4. The metal mass was the total of U and Pu calculated from the hydrogen evolution applying (1) for U and (2) for Pu, respectively. In the calculation, the Pu/U ratio of the initial pellet was applied, since the analysis using XMA showed no significant difference in the Pu/U ratio between the reduced pellet and the initial SIM MOX pellet, as mentioned later. The reduction yield was defined as

$$\text{reduction yield (\%)} = \text{(metal mass)/(total mass of actinoides)} \times 100. \quad (4)$$

The total mass of actinoides in the sample was analyzed using the aqueous solution that was obtained after the determination of the reduction yield. The reduction yield was greater than 90% for all the samples, which were taken from various parts of the reduced pellet. The value was slightly lower than 100% but still high enough to indicate that the major part of the pellet was reduced to metal.

3.4. Observation of the Reduced Pellet

Figure 4 shows a typical back scattering electron (BSE) image of the cross section of the reduced pellet. No remarkable difference was observed between the pellets of RUN 1 and RUN 2. Lots of grains in various sizes looked connected, and porous material was formed over the cross section. The pores in the reduced pellets, which are the black region in the BSE image, must develop due to the significant decrease in the molar volume from oxides to metal, for instance from 24.6 cm^3/mol for UO_2 to 12.4 cm^3/mol for U metal [15].

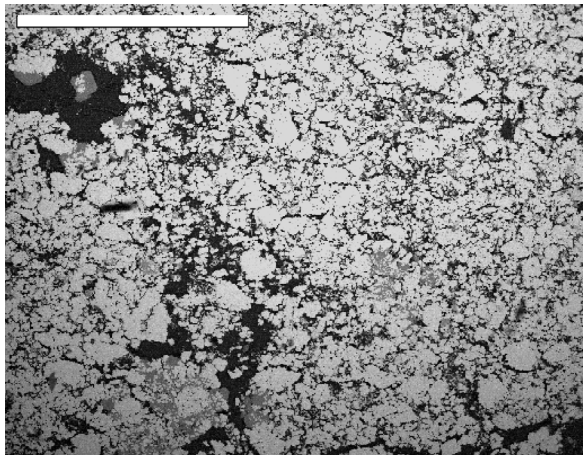

Fig. 4. Back scattering electron image of the cross section of the reduced pellet. The white bar indicates 1 mm in length.

In Fig. 4, light and dark regions of the BSE image were observed clearly. Figure 5 shows a magnified BSE image together with the characteristic X-ray images. Most of U and Pu distributed in the light region of the BSE image and the characteristic X-ray spectrum showed that the light region consisted of U and Pu mainly. The average value of the local Pu/U ratio was 0.101 ± 0.013 for RUN 1 and 0.104 ± 0.017 for RUN 2, respectively, which corresponded with 0.109 ± 0.020 for the archive pellet. These results mean that most of U and Pu formed the alloy by Li reduction without a significant change in the ratio and that the light region should be the alloy.

Figure 5 also shows that most of Ce, Nd, and Sm aggregated in the dark region. The composition analysis by XMA revealed that the main components, 50–80 wt% of the dark region, were the RE elements. The distribution of oxygen was also examined by means of line scanning of the characteristic X-ray. Figure 6 shows the intensity of the X-rays of U, Ce, and oxygen on the arrow indicated in Figure 5. The X-rays of U and Ce were intensive in the light and dark regions in the BSE image, respectively. Although the X-ray of oxygen was relatively close to the back ground level, it was found that oxygen existed with Ce. Thus the RE elements remained oxides as expected from the thermodynamic data showing that the oxygen potential of the RE elements are lower than that of Li.

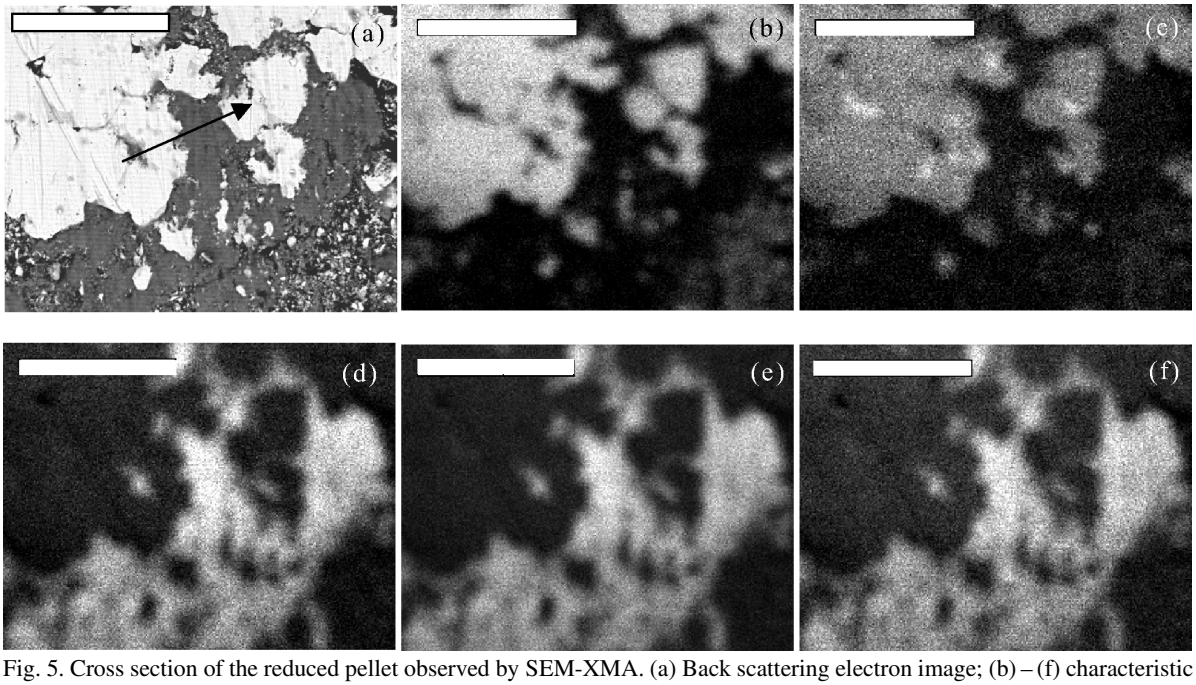

Fig. 5. Cross section of the reduced pellet observed by SEM-XMA. (a) Back scattering electron image; (b) – (f) characteristic X-ray images of U, Pu, Ce, Nd, and Sm, respectively. The white bar in the figures indicates 50 μm in length.

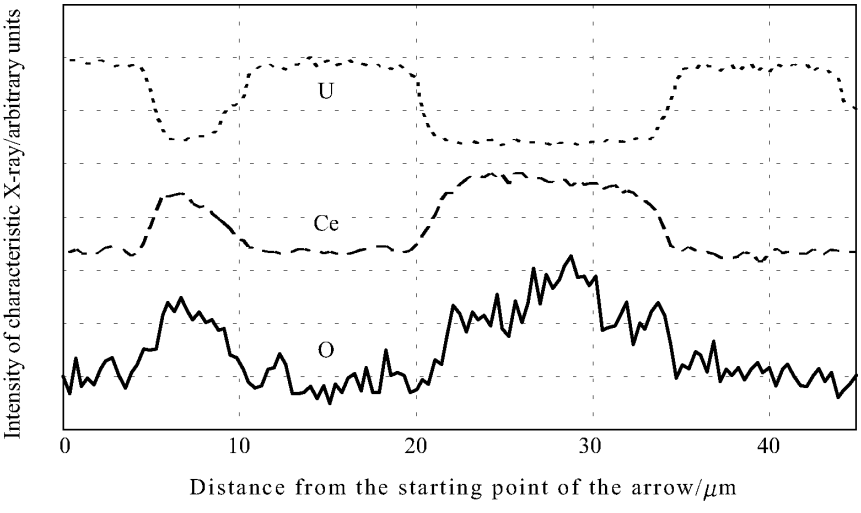

Fig. 6. Intensity of characteristic X-ray of U, Ce, and O on the arrow shown in Figure 5.

Considering the crystal structure similarity among the RE oxides, they should form a solid solution in the aggregation.

The compound, mainly consisting of Pd and Pu, was also found in the reduced pellet. Figure 7 shows the characteristic X-ray images of Pu and Pd together with the BSE image. Spots of Pd were observed, where the characteristic X-ray of Pu was more intense than that in the other area. The composition analysis by XMA indicated that the two elements account for 70 – 90 wt% of the components in the spot. Since Pd must be reduced to metal even in sintering the SIM MOX pellet in argon/3 wt% hydrogen due to its high oxygen potential, Pu and Pd in the spot should form the intermetallic compounds shown in the Pu-Pd binary phase diagram [17]. Since the molar ratio of Pd/Pu was found to be around 1.2, the compounds were considered to be Pu_4Pd_5 or Pu_5Pd_4 rather than $PuPd_3$.

Table 5. Material balance of actinoides.

	U / mg (%)[a]	Pu / mg (%)[a]	Am / mg (%)[a]	Np / mg (%)[a]	Cm / μg (%)[a]
RUN 1:					
(a) Initial loaded	7316	880	13.8	38.3	5.33
(b) Total detected in analysis, (i)+(ii)+(iii)	N. A.[b]	874 (99)	14.1 (103)	39.6 (103)	5.21 (98)
(i) In reduced pellet	7298 (100)	830 (94)	13.0 (94)	39.2 (102)	5.07 (95)
(ii) In molten salt	N. D.[c]	0.9 (0.1)	0.07 (0.5)	0.03 (0.08)	0.01 (0.2)
(iii) In precipitate	18 (0.2)	44 (5)	1.1 (8)	0.3 (0.8)	0.12 (2)
RUN 2:					
(a) Initial loaded	7382	896	14.0	39.8	5.03
(b) Total detected in analysis, (i)+(ii)+(iii)	N. A.[b]	891 (99)	14.4 (103)	39.3 (99)	5.15 (102)
(i) In reduced pellet	7346 (100)	873 (97)	13.8 (99)	38.8 (99)	5.03 (100)
(ii) In molten salt	N. D.	3 (0.3)	0.3 (2)	0.08 (0.2)	0.07 (1)
(iii) In precipitate	36 (0.5)	15 (2)	0.4 (3)	0.4 (1)	0.05 (1)

[a] Values in parenthesis indicate ratio to (a). [b] N. A., not analyzed. [c] N. D., not detected.

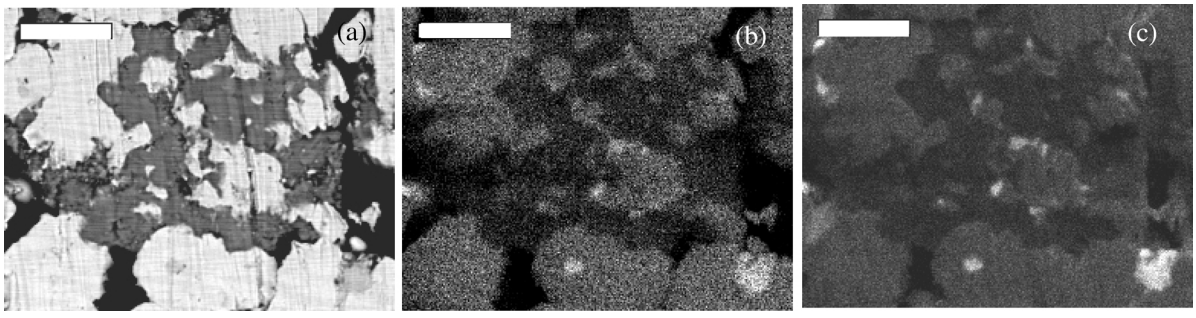

Fig. 7. Cross section of the reduced pellet observed by SEM-XMA. (a) Back scattering electron image; (b) and (c) characteristic X-ray image of Pu and Pd, respectively. The white bar in the figures indicates 20 μm in length.

3.5. Material Balance and Distribution of Each Element

Distribution of Actinoides

The material balances of actinoides are shown in Table 5. The remaining U in the reduced pellet, i. e. (i) in Table 5, was evaluated by subtracting the leaching amount, i. e. (ii) + (iii), from (a) initial loaded, which was originally contained in the SIM MOX. The other elements in the reduced pellet were calculated by normalizing against U on the basis of the composition of the reduced pellet. The value in parentheses in the table indicates the ratio to (a) initial loaded. The total detected in the analysis, i. e. (b) in the table, is around 100% to the initial loaded with ±3% of error for every actinoide, which indicates that good material balance was obtained.

The major part of the actinoides remained in the reduced porous pellet. Meanwhile, a small fraction of the actinoides leached from the pellet and moved to the molten salt or the precipitate on the crucible bottom. The ratio of the leaching, i. e. (ii) + (iii) in Table 5, to the initial loaded was found to be different for each actinoide. It indicates that actinoides leached from the pellet selectively. In this study, the leaching ratio of Am remained at several percent of the initial loaded, compared with about 80% in the previous MOX reduction with U, Pu, and Am [11]. The difference suggests that the existence of fission products suppressed the actinoides leaching, and that a large part of Am in the pellet actually existed in the RE oxide phase rather than in the reduced U-Pu alloy. Considering the crystal structure similarity of RE and Am oxides, it is likely that Am is captured in the solid solution of RE oxides, which formed inside the reduced pellet as mentioned above, to reduce the leaching out of the pellet.

The transuranium elements were detected in the molten salt, while U was not detected in the molten salt. Figure 8 shows the variation of the Pu and Am contents in the salt samples taken during RUN 2. The content increased and decreased repeatedly in the reduction proceeding, and then they settled into almost constant values at the end of the reduction. It seemed that they dissolved into the molten LiCl bath in the presence of oxide ions as a small amount of RE elements dissolved in molten LiCl-Li_2O [12]. As shown

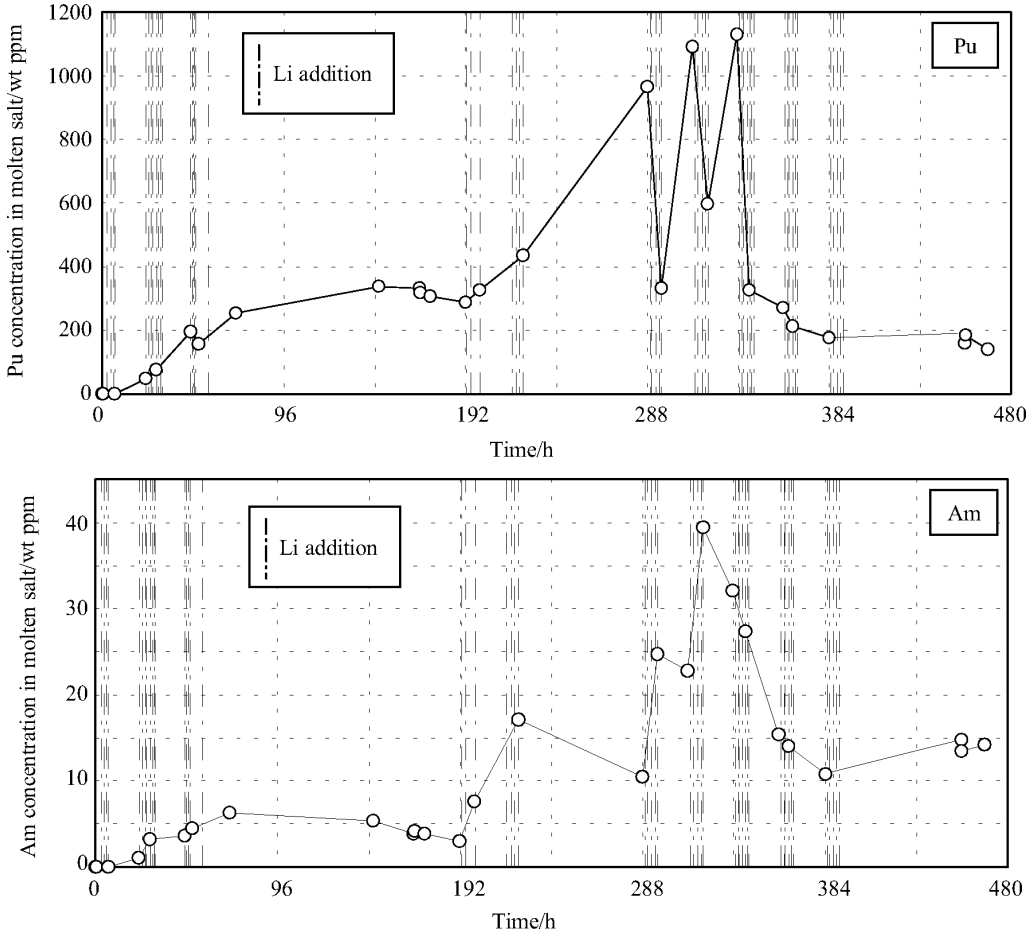

Fig. 8. Content of Pu and Am in the molten salt during RUN 2.

Table 6. Actinoide content in molten salt at the end of the Li reduction.

	Li_2O / wt%	Pu / wt ppm	Am / wt ppm	Np / wt ppm	Cm / wt ppb
RUN 1	1.8	9.0	0.66	0.30	0.12
RUN 2	7.5	150	14	4.0	3.0

in Table 5, the ratio of (ii), i. e. "in molten salt", to the initial loaded is different for each actinoide, and the value is large in the order Am, Cm, Pu, and Np in both RUN 1 and RUN 2. Table 6 indicates the actinoide contents in the molten salt at the end of RUN 1 and RUN 2. The content of each actinoide increased with increasing Li_2O content, since it is higher in RUN 2 (7.5 wt% Li_2O) than in RUN 1 (1.8 wt% Li_2O).

Some of the actinoides precipitated on the crucible bottom. It is considered that part of the actinoides moved into the molten salt inside the pellet, where the Li_2O concentration is higher than that outside the pellet, and then diffused out of the pellet to precipitate at a lower Li_2O concentration. In RUN 2, the salt included in the porous reduced pellet was analyzed for Li metal and Li_2O, as the sample of the pellet was washed in water. The content of Li_2O in the salt was (12.7 ± 2.2) wt%, which was higher than (7.5 ± 0.13) wt% in the bulk of the molten salt bath at the end of RUN 2.

Distribution of Simulated Fission Products

The material balance of RE elements is shown in Table 7. The total detected in the analysis is 100% to the initial loaded with $\pm 3\%$ of error for every RE element. Thus good material balance was also obtained for the RE elements. As for the leaching ratio to the initial loaded, i. e. (ii) + (iii) in Table 5 and Table 7,

	Ce / mg (%)[a]	Nd / mg (%)[a]	Sm / mg (%)[a]
RUN 1:			
(a) Initial loaded	43.2	43.8	39.7
(b) Total detected in analysis, (i)+(ii)+(iii)	42.8 (99)	44.5 (102)	39.7 (100)
(i) In reduced pellet	30.1 (70)	36.1 (82)	23.6 (59)
(ii) In molten salt	8.6 (20)	6.1 (14)	13.3 (34)
(iii) In precipitate	4.1 (9)	2.3 (5)	2.8 (7)
RUN 2:			
(a) Initial loaded	45.9	43.7	40.7
(b) Total detected in analysis, (i)+(ii)+(iii)	45.8 (100)	44.6 (102)	40.1 (99)
(i) In reduced pellet	33.6 (73)	37.3 (85)	31.7 (78)
(ii) In molten salt	8.6 (19)	4.2 (10)	5.0 (12)
(iii) In precipitate	3.7 (8)	3.2 (7)	3.5 (9)

Table 7. Material balance of RE elements.

[a] Values in parenthesis indicate ratio to (a).

	Li_2O / wt%	Ce / wt ppm		Nd / wt ppm		Sm / wt ppm
		This work	Ref. solubility [12]	This work	Ref. solubility [12]	This work
RUN 1	1.8	96	480	69	130	150
RUN 2	7.5	400	2000	200	550	230

Table 8. Content of RE elements in the molten salt at the end of the Li reduction.

	Ba / mg (%)[a]	Pd / mg (%)[a]	Zr / mg (%)[a]	Mo / mg (%)[a]
RUN 1:				
(a) Initial loaded	44.8	46.7	46.7	46.6
(b) Total detected in analysis, (i)+(ii)+(iii)	43.9 (98)	37.3 (80)	42.7 (91)	31.9 (69)
(i) In reduced pellet	0.36 (0.8)	37.3 (80)	36.0 (77)	31.3 (67)
(ii) In molten salt	43.4 (97)	N. D.[b]	N. D.	N. D.
(iii) In precipitate	0.2 (0.4)	N. D.	6.6 (14)	0.6 (0.1)
RUN 2:				
(a) Initial loaded	45.5	47.2	47.1	47.0
(b) Total detected in analysis, (i)+(ii)+(iii)	41.2 (90)	45.3 (96)	41.2 (88)	31.7 (67)
(i) In reduced pellet	0.9 (2)	45.3 (100)	30.3 (64)	30.0 (64)
(ii) In molten salt	40.1 (88)	N. D.	1.5 (3.6)	0.02 (0.04)
(iii) In precipitate	0.2 (0.4)	N. D.	9.5 (20)	1.7 (4)

Table 9. Material balance of Ba, Pd, Zr, and Mo.

[a] Values in parenthesis indicate ratio to (a).
[b] N. D., not detected.

the leaching of the RE elements was larger than that of the actinoides. The leaching ratio indicates that the RE elements also leached from the pellet selectively.

Table 8 indicates the content of the RE elements in the molten salt depending on the Li_2O content. The content of the RE elements increased with increasing Li_2O content as reported for the solubility of Ce and Nd in molten LiCl-Li_2O [12]. Table 8 also shows the reference solubility of Ce and Nd, which was interpolated at the Li_2O contents of 1.8 wt% and 7.5 wt% using the reported solubility data. The contents in this study were lower than the references. While the reference solubility of Ce and Nd was determined in the individual measurement, respectively, multi elements coexisted and the solid solution of RE oxides formed in this study. The chemical activity of the RE elements should decrease in such a solid solution, and then their concentration in the molten salt is considered to decrease compared with the individual solubility.

The material balance of the other simulated fission products is shown in Table 9. Most of Ba distributed in the molten salt bath in both RUN 1 and RUN 2. In molten LiCl-Li_2O, Ba is more stable as chloride, $BaCl_2$, than oxide, BaO, as indicated by [16]

$$\begin{aligned} &BaO + 2LiCl \rightarrow BaCl_2 + Li_2O, \\ &\Delta G = -59.6\ \text{kJ at } 923\ \text{K}. \end{aligned} \tag{5}$$

Because of the wide range solubility of $BaCl_2$ at 923 K in $BaCl_2$-LiCl eutectic quasi-binary system [18], Ba in the spent oxide fuel is considered to essentially dissolve in the molten salt bath of Li reduction.

Almost all of Pd remained in the reduced pellet, and no leaching of Pd was detected. Some amount of Zr and Mo leached from the reduced pellet. Especially, the ratio of Zr in the precipitate to the initial loaded, (iii) in Table 9, is largest among the twelve elements.

4. Conclusions

A simulated spent oxide fuel in a sintered pellet form, which contained the twelve elements U, Pu, Am, Np, Cm, Ce, Nd, Sm, Ba, Zr, Mo, and Pd, was reduced

with Li metal in a molten LiCl bath at 923 K, and the behaviour of each element in the multi-element system was discussed.

The pellet was reduced to become porous, but it remained intact. A shiny metallic colour was observed on the whole cross section of the pellet. Most of U and Pu remained in the pellet to form a porous alloy without significant change in the Pu/U ratio during the reduction. The reduction yield of U and Pu was more than 90%, which was determined using a gas burette to measure the H_2 evolution in dissolving small pieces of the pellet in hydrobromic acid. A small fraction of Pu in the pellet combined with Pd to form stable alloys. Another solid phase in the pellet was observed in the gap of the porous U-Pu alloy and found to be a solid solution of the RE elements, which remained oxide as expected from the oxygen potential of Ce, Nd, Sm, and Li.

Some amount of the RE elements and a small fraction of the actinoides leached from the pellet and moved to the molten LiCl bath or the precipitate on the crucible bottom. Since the ratio of leaching to the initially loaded amount was different for each element, the RE elements and actinoides were found to leach from the pellet selectively. The leaching ratio of Am was only several percent to the initial loaded, which was far from about 80% obtained in previous studies on simple MOX including U, Pu, and Am. The difference suggests that the existence of fission products suppressed the actinoides leaching, and that a large part of Am in the pellet actually existed in the RE oxide phase rather than in the reduced U-Pu alloy.

The detection of the RE elements and actinoides in the molten LiCl bath seemed to indicate that they dissolved into the molten LiCl bath in the presence of oxide ions, which are the by-product of the reduction, as the solubility of the RE elements was measured in molten LiCl-Li_2O previously. Most of Ba also dissolved in the molten salt; on the other hand, no leaching of Pd, which formed stable alloys with Pu in the pellet, was detected.

Acknowledgements

This work was conducted at Harwell, Building 220. The authors gratefully acknowledge the staff of the building, which is being decommissioned, for their warm support.

[1] T. Inoue and H. Tanaka, in: Proceedings of the International Conference on Future Nuclear Systems (GLOBAL 1997), Yokohama, Japan, October 5 – 10, 1997, PV 1, p. 646.
[2] Y. I. Chang, Nucl. Technol. **88**, 129 (1989).
[3] T. Koyama, M. Iizuka, Y. Shoji, R. Fujita, H. Tanaka, T. Kobayashi, and M. Tokiwai, J. Nucl. Sci. Technol. **34**, 384 (1997).
[4] M. Iizuka, K. Uozumi, T. Inoue, T. Iwai, O. Shirai, and Y. Arai, J. Nucl. Mater. **299**, 32 (2001).
[5] K. Uozumi, M. Iizuka, T. Kato, T. Inoue, O. Shirai, T. Iwai, and Y. Arai, J. Nucl. Mater. **325**, 34 (2004).
[6] T. Kato, T. Inoue, T. Iwai, and Y. Arai, J. Nucl. Mater. **357**, 105 (2006).
[7] G. K. Johnson, R. D. Pierce, D. S. Poa, and C. C. McPheeters, in: Actinoide Processing: Methods and Materials (Ed. B. Mishra), The Minerals, Metal & Materials Society, Warrendale, Pennsylvania 1994, p. 199.
[8] T. Usami, M. Kurata, T. Inoue, H. E. Sims, S. A. Beetham, and J. A. Jenkins, J. Nucl. Mater. **300**, 15 (2002).
[9] T. Usami, T. Kato, M. Kurata, T. Inoue, H. E. Sims, S. A. Beetham, and J. A. Jenkins, J. Nucl. Mater. **304**, 50 (2002).
[10] T. Usami, T. Kato, M. Kurata, T. Inoue, H. E. Sims, S. A. Beetham, and J. A. Jenkins, in: Proceedings of the International Conference on Future Nuclear Systems (GLOBAL 2001), Paris, France, September 8 – 12, 2001, FP164.pdf.
[11] T. Usami, T. Kato, M. Kurata, T. Inoue, H. E. Sims, and J. A. Jenkins, J. Nucl. Sci. Technol. Suppl. **3**, 858 (2002).
[12] K. V. Gourishankar, G. K. Johnson, and I. Johnson, Metall. Mater. Trans. B **28**, 1103 (1997).
[13] F. E. Butler and R. M. Hall, Anal. Chem. **42**, 1073 (1970).
[14] N. A. Talvitie, Anal. Chem. **44**, 280 (1972).
[15] J. J. Katz, G. T. Seaborg, and L. R. Morss, The Chemistry of the Actinoide Elements, Chapman and Hall, London 1986.
[16] Japan Calorimetry Society, Thermodynamic Data Base MALT-II, Kagaku-gijutsusya 1992.
[17] T. B. Massalski, in: Binary Alloy Phase Diagrams, 2nd ed., ASM International, Materials Park, Ohio 1990.
[18] E. M. Levin, C. R. Robbins, and H. F. McMurdie, in: Phase Diagrams for Ceramists, vol. 1, The American Ceramic Society, Columbus, Ohio 1964.